 CMES, vol.93, no.4, pp.253-276, 2013

Hyper-Singular Dual Reciprocity Formulation for Potential Problems

C. F. Loeffler[1], **R. G. Peixoto**[2]

Abstract: Here is presented a formal deduction for the Dual Reciprocity hyper-singular boundary integral equation for application to two dimensional potential problems. The theoretical and numerical derivations are presented in detail, and some simple test problems are included to verify the accuracy of the proposed formulation. Due to its simplicity, Poisson's Equation is used as a basis for the mathematical formulations and operational procedures related to the body force term, but the methodology can easily be extended to other more elaborate classes of potential problems. Poles are inserted internally to improve the interpolation within the domain, resulting in a hybrid singular and hyper-singular matrix system and global polynomial functions are also implemented for the same purpose. Problems belonging to scalar field theory that have known analytical solutions are solved, in order to obtain a preliminarily assessment of the efficiency and capability of the technique for more elaborate applications.

Keywords: Dual Reciprocity Formulation; Hyper-singular Integral Formulation; Scalar Potential Problems

1 Introduction

In many problems it is important to know the directional derivatives of the basic variable on the boundary. In elasticity problems, spatial derivatives of displacements are of great interest in order to calculate accurately tangential stresses. In scalar problems many applications require the determination of the velocity field from a given potential pressure, knowledge of both normal and tangential velocity components being essential. For both cases, the objective can be attained through the use of the so-called hyper-singular formulation (HSF) of the Boundary Element Method (BEM).

[1] DEM/PPGEM, Federal University of Espírito Santo, Brazil.
[2] SAMARCO MINERAÇÃO, Brazil.

Despite the high order singularity that appears, the procedure is very useful in the BEM context. The success of the HSF is notable for solving problems involving contact and fracture mechanics. In both cases strong gradients are found, motivating the development of a formulation that offers better precision for the calculation of the spatial derivatives, and at the same time generates two distinct integral equations to represent particles located at the same point, as in the case of a crack. In this situation, one equation is given by the classic BEM formulation (CSF) and the other by the HSF. Similar situation occurs in plate problems, in which it is necessary to write an additional hyper-singular boundary integral equation corresponding to the derivative of the displacement.

Due to this, the HSF has been the subject of considerable research seeking mathematical improvement, considering the concept of the finite part integral [Hildenbrand and Kuhn (1992)], aspects concerning the formulation [Telles and Prado (1993)], proper evaluation of the hyper-singularity [Mantic and Paris (1995); Guiggiani (1995)] and also error analysis [Paulino, Menon and Mukherjee (2001)]. Mansur, Fleury and Azevedo (1997) is of particular importance in which extensive work was done and a thorough approach to the convergence of hyper-singular integrals was developed. At the same time, the technique has been applied to several other important problems in engineering, such as: Darcy's flow, electroplating [Gray and Manne (1993)], wave scattering and the analysis of crack surfaces [Beltrame and Burais (2002)] including anisotropy and plasticity [Shiah and Shih (2007)]. A comprehensive perspective on the current status of HSF with emphasis in regularization procedures is given by Chen and Hong (1999).

The classic Dual Reciprocity Boundary Element Formulation (DRSF) was proposed by Nardini and Brebbia (1982) as an interesting alternative for solving problems modeled by non homogeneous differential equations, which correspond physically to the presence of body forces. With the development of the DRSF, the modeling of body forces becomes easier, since it uses auxiliary interpolation functions that allow transforming domain integrals into boundary integrals accompanied by a point function. Poisson type problems, transient problems, dynamic and wave propagation problems and diffusive-advective problems can also be successfully solved by this approach [Partridge, Brebbia and Wrobel (1982); Ramachandran (1994)]. Due the consistency of the DRSF, beyond these classic situations, it has been continuously applied to new engineering problems [Yun and Ang (2010); Dehghan and Ghesmati (2010); Useche and Albuquerque (2012)].

Despite the suitability of the dual reciprocity to solve domain integrals, its use in some hyper-singular BEM problems has been deprecated by other techniques. For example, the Helmholtz equation comprises an important class of potential problems in which hyper-singular formulation and particular techniques to solve domain

integrals commonly had been applied together, as did Chen and Wong [1998] for the acoustic problem of a cavity using the Multiple Reciprocity Method (MRM). The MRM is a generalization of the concept of the Galerkin vector and treats the domain integral in a recurrence manner, although applying the reciprocity theorem such as is done with the Dual Reciprocity Method [Nowak and Partridge, 1992]. However, the idea behind the MRM and the DRSF are essentially different, since the latter is based on a primitive radial basis interpolation function that allows the domain integral to be changed to boundary integrals.

In fact, the Dual Reciprocity hyper-singular (DRHF) does not appear as the main focus, but as an ancillary tool in a few papers. Cheng et al [2000] indicates it for mixed boundary value problems, while Ang [2007] applies it to a viscoelastic problem. However, important conceptual and numerical aspects were not approached together.

Finally, just based on direct analogy, there is the expectation that the DRHF matrix arrangement is similar to the DRSF. However, it is necessary to demonstrate mathematically that really this analogy is admissible, since it is required a non trivial treatment of the hyper-singularities that also involve the interpolation functions. Thus, this work is intended to present the steps that comprise the mathematical foundations of the DRHF. Moreover, its performance is evaluated solving simple problems, in absence of other factors that may disguise its numerical characteristics.

2 Basic Integral Equations

Let $\Omega(\mathbf{X})$ be a domain in the two dimensional space $\mathbf{X}(x_1, x_2)$, physically homogeneous and isotropic, where a scalar potential variable $u(\mathbf{X})$ is defined and there are known body forces $p(\mathbf{X})$ applied. Thus, consider this field being governed by a Poisson's Equation. Related to this problem, an integral inverse form for a source point ξ located inside the domain can be deduced [Brebbia, Telles and Wrobel (1984)]:

$$u(\xi) - \oint_{\Gamma(\mathbf{X})} u^*(\xi;\mathbf{X}) q(\mathbf{X}) d\Gamma + \oint_{\Gamma(\mathbf{X})} u(\mathbf{X}) q^*(\xi;\mathbf{X}) d\Gamma = - \int_{\Omega(\mathbf{X})} p(\mathbf{X}) u^*(\xi;\mathbf{X}) d\Omega \quad (1)$$

In the previous equation, $q(\mathbf{X})$ is the normal derivative (hereafter denominated flux for simplicity) and was used as an auxiliary function, $u^*(\xi;X)$, called the fundamental solution, and its normal derivative $q^*(\xi;X)$, both related to the Euclidian distance between the field points $\mathbf{X}$ and the source points ξ. These functions are easily found in the specialized literature [Wrobel and Aliabadi (2002)], as well as their analytical expressions. Essential and natural boundary conditions can be

imposed on Γ(X), being given respectively by:

$$u(\mathbf{X}) = \bar{u}(\mathbf{X}) \text{ on } \Gamma_u \tag{2}$$

$$q(\mathbf{X}) = \frac{\partial u(\mathbf{X})}{\partial n(\mathbf{X})} = \bar{q}(\mathbf{X}) \text{ on } \Gamma_q \tag{3}$$

In Eq. (3), n is the outward normal unit vector at a boundary point, and the complete boundary is defined by $\Gamma_u + \Gamma_q$. Values of normal potential derivatives at source points ξ located internally can be easily obtained as follows:

$$\frac{du(\xi)}{dn(\xi)} = \oint_{\Gamma(\mathbf{X})} g^*(\xi;\mathbf{X}) q(\mathbf{X}) d\Gamma - \oint_{\Gamma(\mathbf{X})} p^*(\xi;\mathbf{X}) u(\mathbf{X}) d\Gamma - \frac{d}{dn(\xi)} \int_{\Omega(\mathbf{X})} p(\mathbf{X}) u^*(\xi;\mathbf{X}) d\Omega \tag{4}$$

In the previous equation, the following derivatives are introduced:

$$g^*(\xi;\mathbf{X}) = \frac{\partial u^*(\xi;\mathbf{X})}{\partial n(\xi)} = -\frac{1}{2\pi r}\left(\frac{\partial r}{\partial x_i(\xi)}\right) n_i(\xi) = -\frac{1}{2\pi r^2}[x_i(\xi) - x_i(\mathbf{X})] n_i(\xi) \tag{5}$$

$$\begin{aligned} p^*(\xi;\mathbf{X}) &= \frac{\partial q^*(\xi;\mathbf{X})}{\partial n(\xi)} = \left\{ \frac{-1}{\pi r^3}\left(\frac{\partial r}{\partial x_i(\xi)}\right)[x_j(\xi) - x_j(\mathbf{X})] n_j(\mathbf{X}) + \frac{n_i(\mathbf{X})}{2\pi r^2} \right\} n_i(\xi) \\ &= \frac{1}{2\pi \mathrm{r}^4}\left\{ 2[x_i(\xi) - x_i(\mathbf{X})][x_j(\mathbf{X}) - x_j(\xi)] n_i(\xi) n_j(\mathbf{X}) + r^2 n_i(\mathbf{X}) n_i(\xi) \right\} \end{aligned} \tag{6}$$

The normal derivative also could be introduced into the kernel of the domain integral in Eq. (4), but this is not done for convenience.

A similar procedure used with singular BEM, though more elaborate, allows the deduction of the boundary integral equation for the potential derivative considering sources points located on the boundary. An augmented circular boundary $\bar{\Gamma}_\varepsilon$ needs to be considered in a limit analysis, as shown at Fig. (1). Therefore, the complete boundary is given by: $\Gamma_{ext} = \Gamma - \Gamma_\varepsilon + \bar{\Gamma}_\varepsilon$.

For convenience, consider initially the second integral of the right hand side of Eq. (4).

After application of a constant potential u(ξ) around the field, which does not affect the flux q(ξ), and performing a Taylor Series expansion, this integral along $\bar{\Gamma}_\varepsilon$

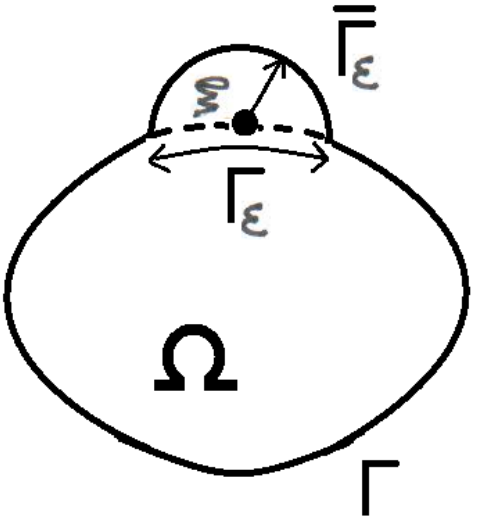

Figure 1: Augmented semicircular domain around the source point ξ.

becomes:

$$\lim_{\varepsilon\to 0}\left[\int_{\bar{\Gamma}_\varepsilon} p^*(\xi;\mathbf{X})[u(\mathbf{X})-u(\xi)]d\Gamma\right] = \lim_{\varepsilon\to 0}\left[\int_{\bar{\Gamma}_\varepsilon}\left(-\frac{1}{2\pi}\right)\frac{[n_i(\mathbf{X})n_i(\xi)]}{\varepsilon}\left(\frac{\partial u(\xi)}{\partial x_j(\xi)}\right)\frac{[x_j(\mathbf{X})-x_j(\xi)]}{\varepsilon}d\Gamma\right] = \lim_{\varepsilon\to 0}\left[-\int_{\theta_\varepsilon}\frac{[n_i(\mathbf{X})n_i(\xi)]}{2\pi}\left(\frac{\partial u(\xi)}{\partial x_j(\xi)}\right)n_j(\mathbf{X})d\theta\right] \tag{7}$$

It must be pointing out that p*(ξ;X) and also g*(ξ;X) lead to simpler expressions when computed on the additional boundary, as introduced in Eq. (7). The complementary integral can be rewritten in CPV sense, since at the ξ point the singularity vanishes, as shown in Eq. (8):

$$\lim_{\varepsilon\to 0}\left[\int_{\Gamma-\Gamma_\varepsilon}[u(\mathbf{X})-u(\xi)]p^*(\xi;\mathbf{X})d\Gamma\right] = CPV\{\oint_{\Gamma}[u(\mathbf{X})-u(\xi)]p^*(\xi;\mathbf{X})d\Gamma\} \tag{8}$$

Similar mathematical treatment must be performed on the first term on the right

hand side of Eq. (3), resulting in the following limit:

$$\lim_{\varepsilon\to 0}\left[\int_{\Gamma-\Gamma_\varepsilon+\bar{\Gamma}_\varepsilon} g^*(\xi;\mathbf{X})q(\mathbf{X})d\Gamma\right] = \lim_{\varepsilon\to 0}\left[\int_{\theta_\varepsilon}\frac{[n_i(\mathbf{X})n_i(\xi)]}{2\pi}\left(\frac{\partial u(\mathbf{X})}{\partial x_j(\mathbf{X})}\right)n_j(\mathbf{X})d\theta\right] + CPV\oint_\Gamma g^*(\xi;\mathbf{X})q(\mathbf{X})d\Gamma \tag{9}$$

The first integral on the right hand side of Eq. (9) has the same value at the limit such as was found by analyzing Eq. (7), and the sum of the two integrals can be computed as a single integral:

$$\begin{aligned}&\lim_{\varepsilon\to 0}\left[\int_{\theta_\varepsilon}\frac{[n_i(\mathbf{X})n_i(\xi)]}{2\pi}\left(\frac{\partial u(\mathbf{X})}{\partial x_j(\mathbf{X})}\right)n_j(\mathbf{X})d\theta\right]\\ &+\lim_{\varepsilon\to 0}\left[\int_{\theta_\varepsilon}\frac{[n_i(\mathbf{X})n_i(\xi)]}{2\pi}\left(\frac{\partial u(\xi)}{\partial x_j(\xi)}\right)n_j(\mathbf{X})d\theta\right]\\ &=\lim_{\varepsilon\to 0}\left[\frac{1}{\pi}\int_{\theta_\varepsilon}[n_i(\mathbf{X})n_i(\xi)]\left(\frac{\partial u(\xi)}{\partial x_j(\xi)}\right)n_j(\mathbf{X})d\theta\right]\end{aligned} \tag{10}$$

This last equation is solved by making an angular integration, but attention must be paid to the fact that $n_i(X)$ is a function of θ. The result of this integral is dependent on the internal angle around the singular point. Therefore, the complete integral can be rewritten in the following form:

$$\begin{aligned}&CPV\{\oint_\Gamma g^*(\xi;\mathbf{X})q(\mathbf{X})d\Gamma-\oint_\Gamma[u(\mathbf{X})-u(\xi)]p^*(\xi;\mathbf{X})d\Gamma\}\\ &-q(\xi)+s(\xi)q(\xi)+w_k(\xi)q_k(\xi)=\frac{d}{dn(\xi)}\int_{\Omega(\mathbf{X})}p(\mathbf{X})u^*(\xi;\mathbf{X})d\Omega\end{aligned} \tag{11}$$

Considering smooth boundaries, $w_k(\xi)$ is zero, $s(\xi)$ is equal to 0.5 and Eq. (11) involves only the flux in the normal direction.

3 Hyper-Singular Dual Reciprocity Formulation

Until now the domain integral related to the source term has remained unchanged. It is interesting operate this term after the substitution of standard DRFS interpolation procedure.

The DRSF interpolates the source function p($\mathbf{X}$) on the domain using commonly a set of radial basis functions F^j [Buhmann (2003)].Then, the inverse integral equation related to the Poisson Equation using DRSF for an internal source point ξ is given by [Partridge, Brebbia and Wrobel (1992)]:

$$u(\xi) - \oint_{\Gamma(\mathbf{X})} u^*(\xi;\mathbf{X})q(\mathbf{X})d\Gamma + \oint_{\Gamma(\mathbf{X})} u(\mathbf{X})q^*(\xi;\mathbf{X})d\Gamma = \alpha^j \left\{ - \oint_{\Gamma(\mathbf{X})} \eta^j(\mathbf{X}^j;\mathbf{X})u^*(\xi;\mathbf{X})d\Gamma + \oint_{\Gamma(\mathbf{X})} \Psi^j(\mathbf{X}^j;\mathbf{X})q^*(\xi;\mathbf{X})d\Gamma + \Psi^j(\mathbf{X}^j;\xi) \right\} \tag{12}$$

In the last expression, α^j are unknown coefficients and ψ^j and η^j are set of primitive functions of F^j, in such a way that it is possible to rewrite the domain integral in terms of the boundary integrals following the same steps used with the Laplace's Equation. It is interesting to note that this procedure avoids problems concerning continuity, attending conditions of differentiation with respect to Cartesian coordinates at all points in the domain, at least for most common radial basis functions used. Moreover, the use of radial functions with high order in the hyper-singular context can more easily induce numerical integration problems.

The choice of interpolating functions F^j is the subject of much research [Zhang and Zhu (1994); Bridges and Wrobel (1996); Partridge (1997); Partridge (2000)]. The general supremacy of one group over the others is very questionable, since the performance of these functions is dependent of many factors. Numerical behavior of certain functions for interpolation or fitting applications can differ as much as the solution of partial differential equations. The mathematical characteristics of the numerical method in which these radial functions are used cannot be neglected. For example, within the BEM context using constant boundary elements, simple radial, spline-plate and cubic radial functions are efficient for solution of Poisson's Equation and Navier's Equation with body forces in two dimensions, as well as other different well known radial functions, since results are found to differ little. However, for problems in three dimensions, the computational experience shows that cubic radial should not be used and many radial functions become inefficient [Bueno (2012)]. Anyway, the choice of best radial basis function is not the focus here.

Deriving Eq. (12) with respect to normal direction n at the point ξ, the following

equation is obtained:

$$q(\xi) - \oint_{\Gamma(\mathbf{X})} g^*(\xi;\mathbf{X})q(\mathbf{X})d\Gamma + \oint_{\Gamma(\mathbf{X})} p^*(\xi;\mathbf{X})u(\mathbf{X})d\Gamma =$$
$$\alpha^j \left\{ - \oint_{\Gamma(\mathbf{X})} \eta^j(\mathbf{X}^j;\mathbf{X})g^*(\xi;\mathbf{X})d\Gamma + \oint_{\Gamma(\mathbf{X})} \Psi^j(\mathbf{X}^j;\mathbf{X})p^*(\xi;\mathbf{X})d\Gamma + \eta^j(\mathbf{X}^j;\xi) \right\} \tag{13}$$

The mathematical treatment for the left hand side of the Eq. (14), in order to take the source point ξ to the boundary, was shown previously. The focus concerns the right hand side of this equation. The same procedure, evaluating the effect of an augmented boundary around the source point ξ is now examined for DRHF integrals. Taking the limit, all the right hand side of Eq. (13) is rewritten as:

$$\alpha^j \left\{ - \oint_{\Gamma(\mathbf{X})} \eta^j(\mathbf{X}^j;\mathbf{X})g^*(\xi;\mathbf{X})d\Gamma + \oint_{\Gamma(\mathbf{X})} \Psi^j(\mathbf{X}^j;\mathbf{X})p^*(\xi;\mathbf{X})d\Gamma + \eta^j(\mathbf{X}^j;\xi) \right\} =$$
$$\alpha^j \left\{ \eta^j(\mathbf{X}^j;\xi) - \lim_{\varepsilon\to 0} \oint_{\Gamma-\Gamma_\varepsilon+\bar{\Gamma}_\varepsilon} \eta^j(\mathbf{X}^j;\mathbf{X})g^*(\xi;\mathbf{X})d\Gamma + \lim_{\varepsilon\to 0} \oint_{\Gamma-\Gamma_\varepsilon+\bar{\Gamma}_\varepsilon} \Psi^j(\mathbf{X}^j;\mathbf{X})p^*(\xi;\mathbf{X})d\Gamma \right\} \tag{14}$$

The second term of the right hand side of the previous expression is better analyzed in two parts, as follows:

$$\begin{aligned} &\lim_{\varepsilon\to 0} \oint_{\Gamma-\Gamma_\varepsilon+\bar{\Gamma}_\varepsilon} \eta^j(\mathbf{X}^j;\mathbf{X})g^*(\xi;\mathbf{X})d\Gamma \\ &= \lim_{\varepsilon\to 0} \int_{\Gamma-\Gamma_\varepsilon} \eta^j(\mathbf{X}^j;\mathbf{X})g^*(\xi;\mathbf{X})d\Gamma + \lim_{\varepsilon\to 0} \int_{\bar{\Gamma}_\varepsilon} \eta^j(\mathbf{X}^j;\mathbf{X})g^*(\xi;\mathbf{X})d\Gamma \end{aligned} \tag{15}$$

The integrability of the first term on the right hand side of Eq. (15) is justified by the kernel of the integral being formed by hyperbolic functions. These functions accompanied by the scalar product [grad(r).(**n**)] show distinct signs before and after the singularity, being self-compensating. Therefore:

$$\begin{aligned} &\lim_{\varepsilon\to 0} \int_{\Gamma_\varepsilon} \eta^j(\mathbf{X}^j;\mathbf{X})g^*(\xi;\mathbf{X})d\Gamma = 0 \rightarrow \lim_{\varepsilon\to 0} \int_{\Gamma-\Gamma_\varepsilon} \eta^j(\mathbf{X}^j;\mathbf{X})g^*(\xi;\mathbf{X})d\Gamma \\ &= \oint_{\Gamma} \eta^j(\mathbf{X}^j;\mathbf{X})g^*(\xi;\mathbf{X})d\Gamma \end{aligned} \tag{16}$$

The second integral on the right hand side of Eq. (15) is related to the increased infinitesimal circular boundary, for which the kernel can be rewritten using simpler coordinates. Thus, considering the former results, Eq. (15) becomes:

$$\lim_{\varepsilon\to 0}\oint_{\Gamma-\Gamma_\varepsilon+\bar{\Gamma}_\varepsilon}\eta^j(\mathbf{X}^j;\mathbf{X})g^*(\xi;\mathbf{X})d\Gamma=\oint_{\Gamma}\eta^j(\mathbf{X}^j;\mathbf{X})g^*(\xi;\mathbf{X})d\Gamma+$$
$$+\lim_{\varepsilon\to 0}\left[\int_{\theta_\varepsilon}\frac{[n_i(\mathbf{X})n_i(\xi)]}{2\pi}\left(\frac{\partial\Psi^j(\mathbf{X}^j;\mathbf{X})}{\partial x_k(\mathbf{X})}\right)n_k(\mathbf{X})d\theta\right] \tag{17}$$

The third term of right hand side of Eq. (14) also needs to be rewritten in two parts: one referred to the augmented region and another concerning the remaining boundary:

$$\lim_{\varepsilon\to 0}\oint_{\Gamma-\Gamma_\varepsilon+\bar{\Gamma}_\varepsilon}\Psi^j(\mathbf{X}^j;\mathbf{X})p^*(\xi;\mathbf{X})d\Gamma$$
$$=\lim_{\varepsilon\to 0}\int_{\Gamma-\Gamma_\varepsilon}\Psi^j(\mathbf{X}^j;\mathbf{X})p^*(\xi;\mathbf{X})d\Gamma+\lim_{\varepsilon\to 0}\int_{\bar{\Gamma}_\varepsilon}\Psi^j(\mathbf{X}^j;\mathbf{X})p^*(\xi;\mathbf{X})d\Gamma \tag{18}$$

The second term on the right hand side of Eq. (18) can be written in the more concisely form. Considering that integration is done exclusively on the increased circular sector and that in this specific region the expression of p*(ξ ;X) is simpler and expanding Ψ^j(X^j;X) in a Taylor Series of first order around ξ , it follows that:

$$\lim_{\varepsilon\to 0}\int_{\bar{\Gamma}_\varepsilon}\Psi^j(\mathbf{X}^j;\mathbf{X})p^*(\xi;\mathbf{X})d\Gamma=$$
$$\lim_{\varepsilon\to 0}\int_{\bar{\Gamma}_\varepsilon}\Psi^j(\mathbf{X}^j;\xi)p^*(\xi;\mathbf{X})d\Gamma+\lim_{\varepsilon\to 0}\left[-\int_{\theta_\varepsilon}\frac{[n_i(\mathbf{X})n_i(\xi)]}{2\pi}\left(\frac{\partial\Psi^j(\mathbf{X}^j;\xi)}{\partial x_k(\xi)}\right)n_k(\mathbf{X})d\theta\right] \tag{19}$$

The hyper singular integral equation for the Poisson problem should properly account for the null effect produced by the introduction of a constant potential u(ξ) such as occurs with Laplace's formulation, where $\nabla^2 u(\xi)=0$. Therefore, taking into consideration the similarity of the mathematical behavior of Laplace's inverse integral form with integrals generated by the Dual Reciprocity procedure, one can conclude that:

$$\lim_{\varepsilon\to 0}\int_{\bar{\Gamma}_\varepsilon}\Psi^j(\mathbf{X}^j;\xi)p^*(\xi;\mathbf{X})d\Gamma=-\lim_{\varepsilon\to 0}\int_{\Gamma-\Gamma_\varepsilon}\Psi^j(\mathbf{X}^j;\xi)p^*(\xi;\mathbf{X})d\Gamma \tag{20}$$

Thus, considering the limit equivalence given by the last expression, the singularity inherent in the first term on the right hand side of Eq. (19), which occurs only when $\xi = \mathbf{X}$, is eliminated. Thus, Eq. (18) can be rewritten in the form given below:

$$\begin{aligned}
&\lim_{\varepsilon\to 0} \oint_{\Gamma-\Gamma_\varepsilon+\bar{\Gamma}_\varepsilon} \Psi^j(\mathbf{X}^j;\mathbf{X}) p^*(\xi;\mathbf{X}) d\Gamma = \oint_{\Gamma} \Psi^j(\mathbf{X}^j;\mathbf{X}) p^*(\xi;\mathbf{X}) d\Gamma + \\
&+ \lim_{\varepsilon\to 0} \left[-\int_{\theta_\varepsilon} \frac{[n_i(\mathbf{X}) n_i(\xi)]}{2\pi} \left(\frac{\partial \Psi^j(\mathbf{X}^j;\xi)}{\partial x_k(\xi)} \right) n_k(\mathbf{X}) d\theta \right]
\end{aligned} \tag{21}$$

Eq. (17) and Eq. (21) replace the two integrals on the right hand side of Eq. (14), namely:

$$\begin{aligned}
&\alpha^j \left\{ \eta^j(\mathbf{X}^j;\xi) - \lim_{\varepsilon\to 0} \oint_{\Gamma-\Gamma_\varepsilon+\bar{\Gamma}_\varepsilon} \eta^j(\mathbf{X}^j;\mathbf{X}) \bar{q}^*(\xi;\mathbf{X}) d\Gamma + \lim_{\varepsilon\to 0} \oint_{\Gamma-\Gamma_\varepsilon+\bar{\Gamma}_\varepsilon} \Psi^j(\mathbf{X}^j;\mathbf{X}) p^*(\xi;\mathbf{X}) d\Gamma \right\} \\
&= \alpha^j \left\{ \eta^j(\mathbf{X}^j;\xi) - \oint_{\Gamma} \eta^j(\mathbf{X}^j;\mathbf{X}) g^*(\xi;\mathbf{X}) d\Gamma + \oint_{\Gamma} \Psi^j(\mathbf{X}^j;\mathbf{X}) p^*(\xi;\mathbf{X}) d\Gamma + \right. \\
&- \lim_{\varepsilon\to 0} \left[\int_{\theta_\varepsilon} \frac{[n_i(\mathbf{X}) n_i(\xi)]}{2\pi} \left(\frac{\partial \Psi^j(\mathbf{X}^j;\mathbf{X})}{\partial x_k(\mathbf{X})} \right) n_k(\mathbf{X}) d\theta \right] \\
&\left. - \lim_{\varepsilon\to 0} \left[\int_{\theta_\varepsilon} \frac{[n_i(\mathbf{X}) n_i(\xi)]}{2\pi} \left(\frac{\partial \Psi^j(\mathbf{X}^j;\xi)}{\partial x_k(\xi)} \right) n_k(\mathbf{X}) d\theta \right] \right\}
\end{aligned} \tag{22}$$

The magnitude of the Ψj gradient at the point ξ in the limit when $\varepsilon \to 0$ can be taken as constant, since only its direction varies along the integration into the circular sector θ_ε. With this, it turns out that:

$$\left(\frac{\partial \Psi^j(\mathbf{X}^j;\mathbf{X})}{\partial x_k(\mathbf{X})} \right) n_k(\mathbf{X}) = \left(\frac{\partial \Psi^j(\mathbf{X}^j;\xi)}{\partial x_k(\xi)} \right) n_k(\mathbf{X}) \tag{23}$$

Thus, the last two terms of Eq. (22) can be added, that is:

$$\alpha^j \left\{ \eta^j(\mathbf{X}^j;\xi) - \lim_{\substack{\varepsilon\to 0 \\ \Gamma-\Gamma_\varepsilon+\bar{\Gamma}_\varepsilon}} \oint \eta^j(\mathbf{X}^j;\mathbf{X}) g*(\xi;\mathbf{X}) d\Gamma + \lim_{\substack{\varepsilon\to 0 \\ \Gamma-\Gamma_\varepsilon+\bar{\Gamma}_\varepsilon}} \oint \Psi^j(\mathbf{X}^j;\mathbf{X}) p*(\xi;\mathbf{X}) d\Gamma \right\}$$
$$= \alpha^j \left\{ \eta^j(\mathbf{X}^j;\xi) - \lim_{\varepsilon\to 0} \left[\int_{\theta_\varepsilon} \frac{[n_i(\mathbf{X}) n_i(\xi)]}{\pi} \left(\frac{\partial \Psi^j(\mathbf{X}^j;\xi)}{\partial x_k(\xi)} \right) n_k(\mathbf{X}) d\theta \right] + \right.$$
$$\left. - \oint_\Gamma \eta^j(\mathbf{X}^j;\mathbf{X}) \bar{q}*(\xi;\mathbf{X}) d\Gamma + \oint_\Gamma \Psi^j(\mathbf{X}^j;\mathbf{X}) p*(\xi;\mathbf{X}) d\Gamma \right\} \tag{24}$$

In a final step, the integral along the circular sector should be rewritten in a numerically more operational form. The final result is given by:

$$\lim_{\varepsilon\to 0} \left[\frac{1}{\pi} \int_{\theta_\varepsilon} [n_i(\mathbf{X}) n_i(\xi)] \left(\frac{\partial \Psi^j(\mathbf{X}^j;\xi)}{\partial x_k(\xi)} \right) n_j(\mathbf{X}) d\theta \right] = s(\xi)\eta^j(\mathbf{X}^j;\xi) + w_k(\xi)\eta_k^j(\mathbf{X}^j;\xi) \tag{25}$$

Similarly as mentioned for Eq. (11), previous equation is simplified for smooth boundaries. Through a standard well-known discretization procedure [Brebbia and Dominguez (1998)], a solvable linear system of equations for Poisson Equation is obtained:

$$\mathbf{W}\{\mathbf{u}\} - \mathbf{D}\{\mathbf{q}\} = [\mathbf{W}\Psi - \mathbf{D}\eta]\{\alpha\} = [\mathbf{W}\Psi - \mathbf{D}\eta]\mathbf{F}^{-1}\{\mathbf{p}\} = \{\bar{\mathbf{P}}\} \tag{26}$$

4 Techniques to Improve the Accuracy of Interpolation

The distribution of p($\mathbf{X}$) inside the domain is not well approximated if the interpolation basis points are taken exclusively on the boundary, usually located in such a way as to coincide with the nodal points. A first feature to improve the accuracy of results is simply the introduction of basis points inside the domain, also named poles [Loeffler and Mansur (1987)]. Depending on the way that these poles are implemented, they can also generate internal results for the potential directly.

The introduction of internal basis point with DRHF is important. To execute the interpolation procedure and carry out the calculation of potential values at internal points simultaneously, a strategy was implemented which needs to introduce a singular integral equation instead of the hyper-singular equation, since this latter

requires the definition of flux in a specific direction. In matrix form, this shown below:

$$\begin{bmatrix} \mathbf{W}\ 0 \\ \mathbf{-H}\ \mathbf{I} \end{bmatrix} \begin{bmatrix} u^c \\ u^i \end{bmatrix} - \begin{bmatrix} \mathbf{D}\ 0 \\ \mathbf{-G}\ 0 \end{bmatrix} \begin{bmatrix} q^c \\ 0 \end{bmatrix} = \left[\begin{bmatrix} \mathbf{W}\ 0 \\ \mathbf{-H}\ \mathbf{I} \end{bmatrix} \begin{bmatrix} \Psi^{cc}\ \Psi^{ic} \\ \Psi^{ci}\ \Psi^{ii} \end{bmatrix} - \begin{bmatrix} \mathbf{D}\ 0 \\ \mathbf{-G}\ 0 \end{bmatrix} \begin{bmatrix} \eta^{cc}\ \eta^{ic} \\ 0\quad 0 \end{bmatrix} \right] \begin{bmatrix} \alpha^c \\ \alpha^i \end{bmatrix} \quad (27)$$

W and **D** are hyper-singular sub-matrices and **H** and **G** are singular ones. Other sub-matrices are related to interpolation functions η^j and $\psi^j$and α^j coefficients. This procedure seems to be reasonable; however, loss of accuracy may appear due to matrix conditioning, since different orders of integrals are involved, especially when other scalar field problems are solved, such as diffusive-advective problems.

Moreover, in some cases it is interesting to implement global functions in the BEM, such as indicated by Goldberg and Chen (1994) and Goldberg, Chen, Bowman and Power (1998). This procedure is very effective for simulating constant, linear and other source terms mathematically expressed as low order functions. Partridge and Wrobel (2007) used this approach in a recent BEM application, modeling thermal behavior of skin tumors. In many situations, radial basis functions and global functions may be used together. Such a strategy has gained increased acceptance, since many recent applications of approximation theory use it, especially some meshless techniques [Hickernell and Hon (1999); Wang and Liu (2002)].

Since this procedure is directly related to the interpolation procedure, it can be applied easily with both DRSF and DRHF.

5 Numerical Simulations

5.1 First Example: Vertical rod subjected to gravity

Fig. 2 shows the physical and geometric features of the first example. The length is L, the specific mass is ρ_0, the Young Modulus is E and gravity is g. The rod is taken as uniform and homogeneous.

The governing equation is a one dimensional case of the Poisson Equation, given by:

$$\frac{d^2u}{dx_1^2} = -\frac{\rho_o g}{E} \quad (28)$$

The vertical displacement is given by $u(x_1)$. The boundary conditions are taken such as:

$$u(x_1 = 0) = 0 \quad (29)$$

$$\frac{du(x_1 = L)}{dx_1} = 0 \quad (30)$$

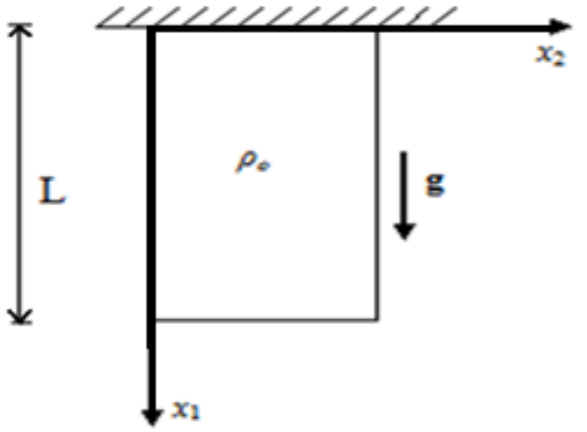

Figure 2: Homogeneous vertical bar subjected to gravity

Numerical results are compared with analytical ones using as a measure the average percentage errors obtained at both internal poles and boundary nodes for displacements and stresses.

Physically the problem is one dimensional, but here it is implemented using a two-dimensional mesh. Thus, the discrete representation of geometry is done taking a square boundary discretized using regular boundary elements. Meshes with 16, 32 and 64 constant boundary elements were used with 0, 4, 9 and 16 internal points uniformly distributed inside the domain. 64 internal points were used exclusively for the more refined mesh.

Values presented are for the cubic radial function. Considering the functions tested, it was this one that produced the better results.

Tab. 1 presents the behavior of the numerical results for displacements with respect to analytical displacement values.

Three meshes with different numbers of poles are considered and the results for the procedure with global interpolation are also included, taking second order global functions (linear and constant terms are included). For this technique, no results for variables located internally are computed. Numerical values for both DRSF and DRHF are presented.

Concerning the results for both formulations, it can be seen that the boundary displacements calculated by the DRSF are better than those obtained by the DRHF. The same occurs on the interior, where the DRSF solution is also better than DRHF

Table 1: Average percentage error for displacements for homogeneous rod

Results for vertical displacements on the boundary and at internal node points							
Number of boundary elements	Number of internal poles	DRSF			DRHF		
		boundary error %	internal error %	global error %	boundary error %	Internal error %	global error %
16 elements	0	3.66	-	3.66	5.05	-	5.05
	4	3.41	2.70	3.23	4.38	2.95	4.03
	9	2.12	1.16	1.71	3.65	1.52	2.74
	global int.	3.68	-	3.68	4.83	-	4.83
32 elements	0	2.08	-	2.08	3.03	-	3.03
	4	1.34	0.79	1.26	2.51	1.70	2.39
	9	0.96	0.33	0.79	2.26	1.26	1.98
	16	1.06	0.43	0.81	2.32	1.36	1.99
	global int.	1.58	-	1.58	1.73	-	1.73
64 elements	0	2.33	-	2.33	2.93	-	2.93
	4	0.75	0.43	0.72	1.53	1.14	1.50
	9	0.56	0.20	0.50	1.36	0.87	1.29
	16	0.47	0.13	0.39	1.30	0.83	1.18
	global int.	0.70	-	0.70	0.75	-	0.75

at internal points. It must be pointed out that displacement values at internal points are more accurate than the boundary values in both formulations.

There is an improvement is accuracy as the mesh is refined as well as with the inclusion of internal points for both formulations, but this latter factor is effective within to a certain limit. Poorest boundary meshes with excessive number of internal poles presented loss of accuracy, probably because the matrices become ill-conditioned.

In this example the global functions performed better with the DRHF than with DRSF. For DRSF, global function results were less accurate than those obtained with the introduction of internal poles. As the gravitational field is constant, it would be represented exactly by the global functions in the case of simple interpolation. However, the Dual Reciprocity procedure requires auxiliary matrices $\boldsymbol{\Psi}$ and $\boldsymbol{\eta}$ which generate additional harmful numerical effects.

Tab. 2 presents the results for stress: tractions on the clamped boundary and axial normal stresses internally. Now the numerical results on the boundary nodes with DRHF are better than singular results. However, the numerical accuracy of the internal stresses with DRSF is still superior to the DRHF results. For the DRHS, the use of global functions was more effective than introduction of internal poles for improving the accuracy of numerical results.

Table 2: Average percentage error for normal stresses for homogeneous rod

Results for normal vertical stresses on the boundary and at internal nodal points							
Number of boundary Elements	Number of internal poles	DRSF			DRHF		
		boundary error %	internal error %	global error %	boundary error %	internal error %	global error %
16 elements	4	2.65	1.54	2.29	1.77	4.43	3.65
	9	2.53	0.68	1.30	1.65	3.22	2.99
	global interp.	3.22	-	3.22	2.37	-	2.37
32 elements	4	1.63	0.52	1.30	1.35	2.28	1.85
	9	1.42	0.22	0.80	1.14	1.77	1.58
	16	1.47	0.34	0.83	1.19	2.00	1.81
	global interp.	2.03	-	2.03	0.80	-	0.80
64 elements	4	0.98	0.27	0.85	0.96	1.23	1.07
	9	0.87	0.14	0.61	0.77	0.98	0.89
	16	0.84	0.08	0.46	0.73	0.94	0.86
	global interp.	1.07	-	1.07	0.75	-	0.75

5.2 Second Example: Vertical rod with variable density submitted to gravity

To analyze the behavior of the proposed formulations when there is a gradient of the body force, a similar problem to the previous one was simulated, but now the density of the rod is considered to vary quadratically with the vertical coordinate. In this case, the differential equation is given by:

$$\frac{d^2u}{dx_1^2} = -\frac{g}{EL^2}\rho_0(L^2 - x_1^2) \tag{31}$$

The same boundary conditions as in the first example were used. Also the meshes are the same as used in the previous simulations. Cubic radial basis functions are taken to interpolate the domain term. Quadratic global functions are also used in tests for comparison.

Tab.3 presents the mean percentage errors in displacements for both boundary and internal nodes for all meshes tested, considering the two formulations discussed.

In this example, numerical results for the displacements by the DRHF also were worse than the results of the DRSF. On the other hand, the global functions now presented the best numerical performance, although not able to approximate exactly the parabolic body force proposed.

Regarding the numerical results for boundary tractions and internal stresses, given in Tab. 4, different from the behavior shown in the previous example, the DRHS

did not produce better results than the DRSF, but both formulations had similar performance.

Table 3: Average percentage error for displacements for the non-homogeneous rod

Results for vertical displacements on the boundary and internal nodal points							
Number of boundary Elements	Number of internal poles	DRSF			DRHF		
		boundary error %	internal error %	global error %	boundary error %	internal error %	global error %
16 elements	4	4.18	3.45	3.99	6.89	7.13	6.95
	9	3.74	2.83	3.35	6.64	6.47	6.57
	global int.	2.98	-	2.98	5.86	-	5.86
32 elements	4	1.68	1.18	1.61	4.49	4.11	4.43
	9	1.51	0.95	1.36	4.37	3.78	4.21
	16	1.51	0.97	1.39	4.36	3.87	4.26
	global int.	1.28	-	1.28	4.12	-	4.12
64 elements	4	1.10	0.81	1.08	2.91	2.67	2.90
	9	0.81	0.52	0.76	2.67	2.27	2.60
	16	0.75	0.42	0.67	2.60	2.23	2.51
	global int.	0.56	-	0.56	2.18	-	2.18

Table 4: Average percentage error for normal stresses for the non-homogeneous rod

Results for normal vertical stresses on the boundary and internal nodal points							
Number of boundary Elements	Number of internal poles	DRSF			DRHF		
		Boundary error %	internal error %	global error %	boundary error %	internal error %	global error %
16 elements	4	4.04	3.33	4.10	3.75	6.35	5.84
	9	4.00	2.73	3.33	3.73	5.60	5.45
	global int.	3.48	-	3.48	3.64	-	3.64
32 elements	4	2.52	1.15	2.16	3.21	3.32	3.53
	9	2.44	0.92	1.69	3.13	2.95	3.21
	16	2.46	0.96	1.50	3.17	3.06	3.22
	global int.	2.17	-	2.17	2.69	-	2.69
64 elements	4	1.73	0.59	1.53	2.46	1.89	2.44
	9	1.63	0.37	1.19	2.20	1.59	2.04
	16	1.52	0.35	0.94	2.14	1.61	1.92
	global int.	1.52	-	1.52	1.15	-	1.15

Based on the Weighted Residual Method [Brebbia, Telles and Wrobel (1984)], there is a preliminary expectation that higher gradients would be better represented by the HSF, since similarly the kernels of integrals have functions with higher reverse order. However, the hyper-singular integral equation is not exactly equivalent to a sentence of weighted residuals as a singular equation, since there is an additional regularization term given by Eq. (8). Thus, these results do not confirm any general conclusions about the adequacy of the hyper-singular approach in Poisson problems, in which basic variables present higher gradients. However, it must be pointing out that the features of radial functions also interfere in the results. They may not be effective to approximate this hyper-singular domain integral particularly.

5.3 Third Example: Prismatic rod of square section submitted to uniform torsion

The third example consists of a prismatic rod of square cross section under uniform torsion, as shown schematically in Fig. 3:

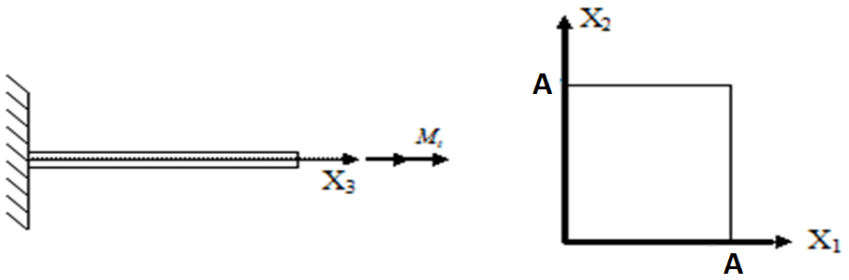

Figure 3: Uniform torsion in a square rod

Partial differential equation governing of this problem is a Poisson Equation, written strategically in terms of a special potential, known as torsion function $u(x_1,x_2)$, such that:

$$\nabla^2 u(x_1,x_2) = -2G\theta \tag{32}$$

In Eq. (32), θ represents the angular displacement per unit length and G is the shear modulus of the constitutive material of the rod. The distribution of shear stresses over the cross section is given by the spatial derivatives for the torsion function, that is:

$$\tau_{x1} = \frac{\partial u(x_1,x_2)}{\partial x_2}; \tau_{x2} = -\frac{\partial u(x_1,x_2)}{\partial x_1} \tag{33}$$

The analytical expression for stresses at each direction is given by:

$$\tau_{xi} = \frac{32G\theta}{a\pi^3} \sum_{m=1,3,\ldots}^{\infty} \sum_{n=1,3,\ldots}^{\infty} [\delta_{i1} \frac{sen\left(\frac{m\pi x_1}{a}\right) cos\left(\frac{n\pi x_2}{a}\right)}{m\left(\frac{m^2+n^2}{a^2}\right)} - \delta_{i2} \frac{cos\left(\frac{m\pi x_1}{a}\right) sen\left(\frac{n\pi x_2}{a}\right)}{n\left(\frac{m^2+n^2}{a^2}\right)}] \tag{34}$$

The values of the shear modulus of the constitutive material of the rod, the angular displacement per unit length and edges **A** are also considered unitary in the simulations. The prescribed condition on all boundaries is the torsion potential equal to zero.

Table 5 presents the results of shear stress at nodal points and internal points. Using constant boundary elements, the difficulty to simulate accurately numerical values at nodal points near the corners is more pronounced. Thus the results for average percentage error are obtained both considering the values at nodal points near the edges and excluding them.

Table 5: Average percentage error for torsion problem

Shear stresses at boundary points and internal points Cubic radial basis functions for body force interpolation									
Number of boundary elements	Number of internal poles	DRSF % error				DRHF % error			
		Int. points	All nodes	Corners excluded	Total	Int. points	All nodes	Corners excluded	Total
16 elements	0	-	10.23	9.18	10.23	-	7.11	6.25	7.11
	4	5.77	9.15	1.78	8.02	4.79	7.17	1.08	6.38
	9	0.92	9.81	3.54	6.00	0.38	6.69	0.61	3.99
	global func.	-	4.14	2.23	4.14	-	5.99	1.78	5.99
32 elements	0	-	6.02	1.09	6.02	-	5.68	0.67	5.68
	4	1.59	5.95	1.13	5.07	1.68	5.16	0.11	4.46
	9	0.32	6.23	1.54	4.62	0.37	5.45	0.52	4.06
	16	0.08	6.20	1.45	3.14	0.20	5.41	0.43	2.80
	global func.	-	3.22	0.89	3.22	-	5.08	0.63	5.08
64 elements	0	-	5.10	1.93	5.10	-	5.68	1.62	5.68
	4	0.89	4.51	1.39	4.10	1.08	4.37	0.19	4.00
	9	0.27	4.87	1.67	4.14	0.38	4.37	0.21	3.74
	16	0.30	4.37	1.45	3.02	0.39	4.46	0.29	3.10
	global func.	-	2.31	0.37	2.31	-	4.19	0.35	4.19

In this case, the implementation of constitutive internal points for the improvement of the interpolation procedure was again effective with respect to accuracy of results for both formulations. However, just for the DRSF model the global functions interpolate more accurately the constant source term than the internal poles, producing the better results.

The most important aspect, however, is that most results obtained with the DRHF have been more accurate than the results obtained with the DRSF. This is even more accurate when the nodal points near the corners are excluded, since it is well known that the hyper-singular formulation results are worse than those of the classical formulation in this region.

In principle, this behavior suggests a better performance of the hyper-singular formulation in the calculation of the normal derivatives. However, computational tests presented some important features related to HSF that prevent such immediate conclusions. It is worth noting that all results are consistent for values of normal derivatives on the boundary, since the potential in this case is prescribed as zero along the entire boundary.

5.4 Fourth Example: S emicircular plate subject to temperature discontinuity

In this problem there is no domain force: the purpose of this example is to show that the regularization term given in the Eq. (8) vanishing can be the main factor to produce best results with the hyper-singular formulation. This effect occurs due to a particular behavior of the potential, such as null or constant values along the boundary.

A semicircular plate of radius 4.0 length units subject to a thermal distribution given in polar coordinates by:

$$u(r) = \frac{\theta}{\pi} \tag{35}$$

As shown in Fig. 4, there is a discontinuity in the prescribed temperature value at r = 0 and the circular boundary is considered to be insulated, that is, q=0.

Thus, the solution for potential derivative along the horizontal edge is a hyperbolic function, singular at x_1=0, as shown by Eq. (36):

$$q(x_1, x_2 = 0) = -\frac{1}{x_1} \tag{36}$$

In this case, thirty two constant boundary elements were used for the discretization.

Results at the nodal points belonging to the curved boundary are similar with both classic and hyper-singular formulations, presenting larger errors at the corners.

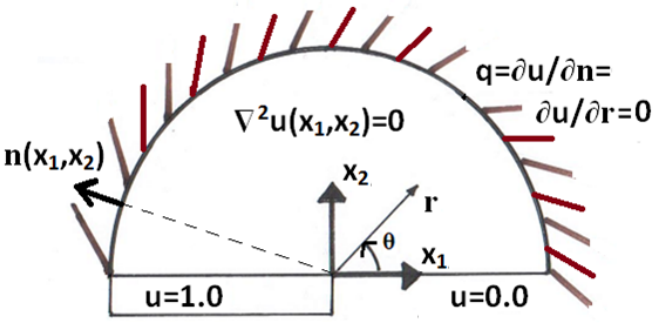

Figure 4: Semicircular plate subject to discontinuity in the temperature on the straight boundary

However, the values obtained for the nodal points along the horizontal line are quite different. The singular formulation produces major errors in the middle, closer to the singularity, while the hyper-singular introduces negligible errors in this sector, as illustrated in Fig. 5, where the dashed line refers to the percentage error of the HSF along the x coordinate, and the full line refers to the same parameter for the CSF. This good behavior of the numerical response in the region near the singularity could suggest the idea that in problems with high gradients, application of the HSF would have a better numerical performance. However, it also should be noted that the term [u(X)-u(ξ)] expressed by Eq. (8) is zero in this case, such as occurred in the torsion problem.

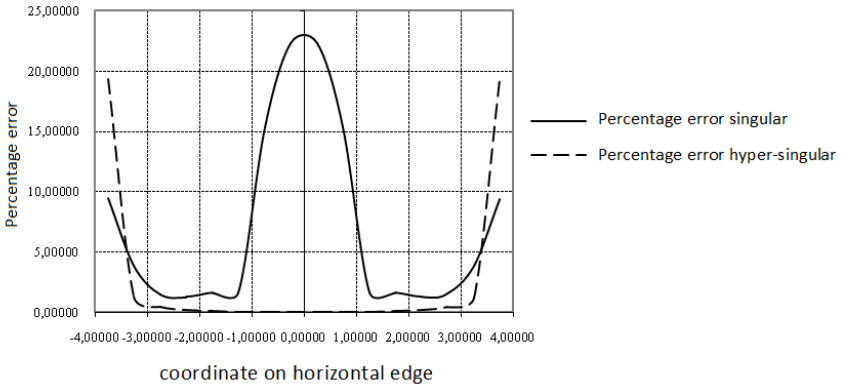

Figure 5: Normal flux percentage error curve along the horizontal edge

6 Conclusions

It was demonstrated mathematically that the Dual Reciprocity technique can be applied in the hyper-singular boundary element formulation. The resulting matrix arrangement is really analogous with the required arrangement of the DRSF, being the standard BEM matrices substituted by hyper-singular ones, ensuring the same ease of computational implementation.

Based on computer simulations presented, the precision of the classic singular formulation is superior for potential results, while the DRHF tends to produce better results for the potential normal derivative. As a matter of fact, this confirms a certain expectation in which the HSF usually tends to reach better performance for the potential normal derivative. However, further studies must still be conducted in order to achieve more general conclusions about this important mathematical aspect, since a closer examination has shown that some problems in which the HSF had very good accuracy special conditions of potential were prescribed. Then, these conditions would favor the convergence of a specific term of the hyper-singular formulation.

The idea that the HSF may have a better performance when the basic variables of the problem present high gradients cannot be confirmed from the simulations presented.

The features of radial interpolation functions, which often do not adapt well to certain body force shapes, should not be disregarded. Particularly, cubic radial functions were chosen here due the better performance. Other different radial basis functions such as simple radial and spline-plate were tested and results were similar. But in many situations may be different, and the proper choice of suitable radial basis functions is important. Concerning the use of global functions, the scheme was reasonably effective, but stood out mainly with the DRHF.

Overall, although the DRHF has not a better performance than the singular formulation, it is feasible to use it in conjunction with the latter to represent static or dynamic body forces, when two integral equations are necessary to describe the mathematical problem. Particularly concerning plate problems, dynamic conditions appear on many civil, mechanical and aerospatial applications, requiring an effective BEM approach to solve domain integrals due to the presence of inertial terms.

References

Ang, W. T. (2007): Elastodynamic antiplane deformation of a biomaterial with an imperfect viscoelastic interface: A dual reciprocity hypersingular boundary integral solution. *Applied Mathematical Modelling,* vol. 31, no. 4, pp. 749-762.

Beltrame, Ph.; Burais, N. (2002): Computing methods of hyper-singular integral applied to eddy-current testing. *IEEE Transactions on Magnetics*, vol.38, no.2, pp. 1269-1272.

Brebbia, C. A.; Domínguez, J. (1998): *The Boundary Element Method – An Introductory Course.* WIT Press.

Brebbia, C. A.; Telles, J.C.; Wrobel, L. C. (1984): *Boundary Element Techniques.* Springer Verlag.

Bridges, T. R.; Wrobel, L. C. (1996): A dual reciprocity formulation or elasticity problems with body forces using augmented thin plate splines. *Communications in Numerical Methods in Engineering,* vol.12, no.3, pp. 209-220.

Bueno, F. R. (2012): Three dimensional inverse analyses using genetic algorithm for the localization of skin tumors using the dual reciprocity method (In Portuguese). PhD. Thesis, University of Brasilia, Civil and Environmental Department.

Buhmann, M. D. (2003): *Radial Basis Functions: Theory and Implementations*, first ed., Cambridge, University Press, New York.

Chen, J. T.; Wong, F. C. (1998): Dual formulation of multiple reciprocity method for the acoustic mode of a cavity with a thin partition. *Journal of Sound and Vibration*, no.217, 75-95.

Chen, J.T.; Hong, H.K. (1999): Review of dual boundary element methods with emphasis on hypersingular integrals and divergent series. *Applied Mechanics Reviews*, vol.52, no.1, pp.7-33.

Cheng, A.H.D.; Young, D.L.; Tsai, C.C. (2000) Solution of poisson's equation by iterative DRBEM using compactly supported, positive definite radial basis function. *Engineering analysis with Boundary Elements,* vol.24, pp.549-557.

Dehghan, M.; Ghesmati, A. (2010): Solution of the second-order one-dimensional hyperbolic telegraph equation by using the dual reciprocity boundary integral equation (DRBIE) method. *Engineering Analysis with Boundary Elements*, vol.34, no.1, pp. 51-59.

Goldberg, M. A.; Chen, C.S. (1994): The theory of radial basis functions applied to the bem for inhomogeneous partial differential equations. *Boundary Elements Communications,* vol.5, pp. 57-61.

Goldberg, M. A.; Chen, C. S.; Bowman, H.; Power, H. (1998): Some comments on the use of radial basis functions in the dual reciprocity method. *Computational Mechanics*, vol.21, pp. 141-148.

Gray, L. J.; Manne, L. L. (1993): Hyper-singular integrals at a corner. *Engineering Analysis with Boundary Elements*, vol. 11, no.4, pp. 327-334.

Guiggiani, M. (1995): Hyper-singular boundary integral equations have an addi-

tional free term. *Computational Mechanics,* vol.16, pp. 245-248.

Hickernell, F. J.; Hon, Y.C. (1999): Radial basis function approximations as smoothing splines. *Applied Mathematics and Computation*, vol. 102, pp.1-24.

Hildenbrand, J. ; Kuhn, G. (1992): Numerical computation of hyper-singular integrals and application to the boundary integral equation for the stress tensor. *Engineering Analysis with Boundary Elements*, vol.10, pp.209-217.

Loeffler, C. F.; Mansur, W. J. (1987): Analysis of time integration schemes for boundary element applications to transient wave propagation problems, in: C.A. Brebbia (Ed.), *Boundary Element Techniques: Applications in Stress Analysis and Heat Transfer, Computational Mechanics Publishing*, UK, 1987, pp. 105-124.

Mansur, W. J.; Fleury, Jr. P.; Azevedo, J. P. S. (1997): A vector approach to the hyper-singular BEM formulation for Laplace's equation in 2D. *International Journal of BEM Communications,* vol.8, pp. 239-250.

Mantic, V.; Paris, F. (1995): On free terms and singular integrals in isotropic and anisotropic potential theory. *Proc. IABEM*, Hawaii.

Nardini, D.; Brebbia, C. A. (1982): A new approach for free vibration analysis using boundary elements, in: C. A. Brebbia (Ed.). *Boundary Element Methods in Engineering*, pp. 312-326.

Nowak, A. J.; Partridge, P. W. (1992): Comparison of the dual reciprocity and the multiple reciprocity methods. *Engineering Analysis with Boundary Elements*, vol. 10, pp.155-160.

Partridge, P. W. (1997): Approximation functions in the dual reciprocity method. *International Journal of Boundary Elements Communications*, vol.8, no.1, pp.1-4.

Partridge, P. W. (2000): Towards criteria for selecting approximation functions in the dual reciprocity method. *Engineering Analysis with Boundary Elements*, vol.24, no.7, pp.519-529.

Partridge, P. W.; Wrobel, L. C. (2007): An inverse geometry problem for the localization of skin tumors by thermal analysis. *Engineering Analysis with Boundary Elements*, vol.10, pp. 803-811.

Partridge, P. W.; Brebbia, C. A.; Wrobel, L. C. (1992): *The Dual Reciprocity Boundary Element Method.* Computational Mechanics Pub.

Paulino, G. H.; Menon, G., Mukherjee, S. (2001): Error estimation using hyper-singular integrals in boundary element methods for linear elasticity. *Engineering Analysis with Boundary Elements*, vol. 25, no.7, pp. 523-534.

Ramachandran, P. A. (1994): *Boundary Element Methods in Transport Phenomena*. Computational Mechanics Publication and Elsevier Applied Science, London.

Shiah, Y. C.; Shih, Y. S. (2007): Regularization of nearly singular integrals in the boundary element analysis for interior anisotropic thermal field near the boundary. *Journal of the Chinese Institute of Engineers*, vol. 30, no. 2, pp. 219-230.

Telles, J. C. F; Prado, A. A. (1993): Hyper-singular formulation for 2-D potential problems, in Aliabadi M.H. and Brebbia C.A. (Eds.). *Advanced Formulations in Boundary Element Method*, Chap. 6, Elsevier, London, cap. 6.

Useche, J.; Albuquerque, E. L. (2012): Dynamic analysis of shear deformable plates using the dual reciprocity method.*Engineering Analysis with Boundary Elements*, vol.36, no.5, pp. 627-632.

Wang, J. G.; Liu, G. R. (2002): A point interpolation meshless method based on radial basis functions. *International Journal for Numerical Methods in Eng.,* vol. 54, pp. 1623-1648.

Wrobel, L. C.; Aliabadi, M. H. (2002): *The Boundary Element Method. C*hichester, Wiley.

Yun, B. I.; Ang, W. T. (2010): A dual reciprocity boundary element approach for axisymmetric nonlinear time-dependent heat conduction in a nonhomogeneous solid. *Engineering Analysis with Boundary Elements*, vol. 34, no. 8, pp. 697-706.

Zhang, Y.; Zhu, S. (1994): On the choice of interpolation functions used in the dual reciprocity boundary-element method. *Engineering Analysis with Boundary Elements,* vol. 13, no.4, pp. 387–396.